SPATIAL SEISMIC EXCITATIONS AND RESPONSE SPECTRA

Zbigniew Zembaty
Opole University of Technology
45-271 Opole ul.Mikolajczyka 5
Poland

ABSTRACT

Formal extensions of the response spectrum method to include spatial seismic effects are reviewed. Two approaches are described in detail: the first based on random vibrations of a simple oscillator under two-component excitations, and the second analyzing multi-column building seismic response. The subjective choice of these two complementing approaches aims at analyzing the phenomenon of spatial seismic vibrations of structures from a broader physical perspective of various wave types propagating among structural supports, with detailed random vibration sensitivity analysis of a simple structural system still included.

KEYWORDS: Response Spectrum, Spatial Seismic Effects, Differential Ground Motion, Wave Propagation, Site Amplification

INTRODUCTION

The question of why, after 75 years, the response spectrum method (Biot, 1932) still captures our attention and ignites our imagination is quite a pertinent one. Two different answers to this question come to mind. On one hand, the response spectrum method in its full form, generalized to multi-degree-of-freedom (MDOF) systems, is quite effective and very early it became a standard tool for engineers designing structures to withstand seismic loads. On the other hand, even for single-degree-of-freedom (SDOF) systems, the conceptual clarity of a simple "mechanical analyzer for the prediction of earthquake stresses" (Biot, 1941) made it a very convenient vehicle for analyzing new structural models for various types of ground motions.

Indeed, in spite of the fact that advanced finite element method (FEM) softwares applying dedicated finite element models and nonlinear procedures can solve many sophisticated structural seismic problems using hundreds of thousands degrees of freedom, our ability to understand and predict structural response under seismic excitations still remains substantially limited. This is partly because the more advanced and extended such modeling becomes, and the greater are the dimensions of the analyzed structural system, the more case-dependent our analysis becomes, and the less general conclusions we can draw. Paradoxically, it seems that the larger we make our model the more we are losing the "big picture" of our problem. So, after all the expensive FEM efforts, we are often left powerless like Pooh Bear from the childish book (*...but to his surprise, the more Pooh Bear, looked inside the house, the more Piglet wasn't there; A.A. Milne: "The House at Pooh Corner"*).

The purpose of this paper is to review one particular aspect of the response spectrum method, namely, its formal extension to include the effects of seismic signal variations along or across the structural dimensions. In this case, the advantage of clear physical interpretation of the response spectrum concept is particularly appealing. It is obvious that the modeling simplifications can lead only to approximate results; yet by reducing the number of parameters to a very few—the most necessary ones—a clearer view of the physics of the analyzed problem may be possible. For many practical engineering situations, these approximations are quite adequate.

SPATIAL SEISMIC EFFECTS ON STRUCTURES

The origin of spatial seismic effects can be attributed to following three main sources:
- complexity of seismic focus,
- finite velocity of wave propagation, and
- geological and geometrical heterogeneities of the ground.

The first source of spatial variability can be particularly important for near-field strong motion, and its effects are still difficult to quantify. The second source depends directly upon the ratio of the longest structural dimension to the shortest significant wavelength. The third source of spatial seismic variability leads on one hand to complicated problems of wave diffraction and interference (see, e.g., Aki and Richards, 1980), and on the other hand to local soil amplification (e.g., Trifunac, 1990; Safak, 1995).

Consider a general multi-support structure (as in Figure 1). The seismic waves propagating along this structure excite the motion of structural foundations with a phase shift depending upon the wavelength and the apparent propagation velocities. It can be seen that in addition to the familiar dynamic response the presence of pseudo-static motion will cause substantial strains in the structure. In a situation in which the excitations act slowly, say with vibration periods $\gg T_1$ (= fundamental period of the structure), the strains in the structure will be caused 'solely' by the asynchronous support movements. Thus, it is the combination of the dynamic vibrations and pseudo-static motions, depending upon the spectral content of excitations and the apparent wave propagation velocities, that will determine the overall structural performance under spatial seismic excitations. One should also note that the differential effects among columns of the structure will always be somewhat reduced by the soil compliance, or more generally, by the soil-structure-interaction (SSI) effects (see the zoomed area of Figure 1).
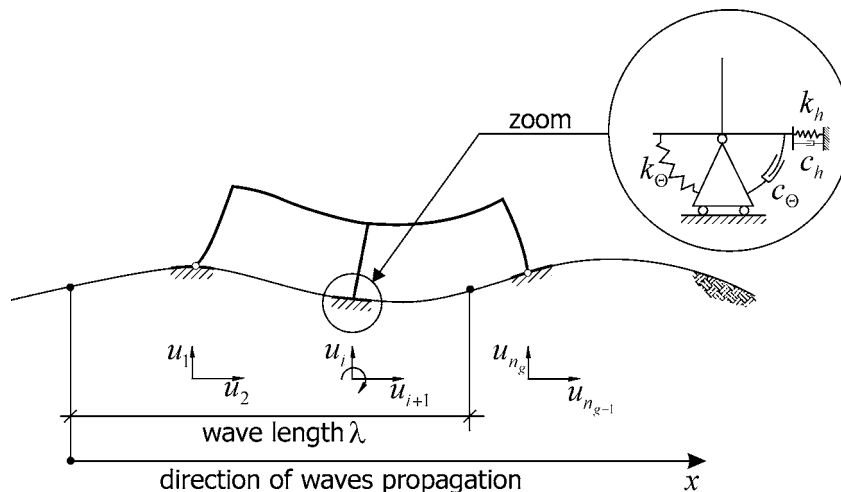

Fig. 1 A structure subjected to multi-support, kinematic wave excitations

The significance and recognition of spatial seismic effects grew following the arrival of experimental evidence since late 1980s, when the records from extended seismic arrays like SMART-1 became available (Abrahamson et al., 1987). From that time the number of journal papers on this subject has increased significantly.

The spatial seismic effects on structures can be analyzed with varying degrees of sophistication. The simplest way to include the effect of spatial seismic effects on a multi-support structure is to simply carry out a time-history analysis with certain seismic record applied to structural supports with some time delay. The time shift among structural supports can be selected so that it reflects the apparent wave velocity in the ground motion. Such an analysis for a typical reinforced concrete bridge structure on multiple supports was described by Leger et al. (1990). Modern computer codes (e.g., ABAQUS) even make it possible to observe the time dependence of a map of particular stresses in the structure as the excitation propagates along the structural supports (Dulinska and Zieba, 2007). Such a simple deterministic analysis can be conceptually clear, but the following aspects of the spatial seismic effects may still not be properly addressed.

The Arbitrary Choice of the Single Apparent Wave Velocity: Theoreticians will note that this approach ignores the fact that there exist multiple apparent wave velocities that also depend upon the frequencies of motion being analyzed and that result from the dispersion in strong-motion waves (Trifunac, 1971).

The Assumption of Uniformity of the Ground Properties along the Structure: In many cases, the ground properties differ among different structural supports. This may be particularly true for the bridges

crossing alluvial valleys with rock outcrops. In such situations, ground motions at different supports of a structure may be very different.

Loss of Coherence among the Motions at the Supports of the Structure: Simultaneous measurements of seismic signals at two distinct points on the ground surface display differences that result from substantial randomness in the medium through which the seismic signal is transmitted. This effect, called loss of coherency, should be taken into account.

Many spatial seismic ground motion models based on the SMART-1 measurements were formulated and analyzed through correlation/coherence functions describing the surface wave field in terms of the random field theory (e.g., Abramhamson and Bolt, 1985; Abrahamson et al., 1991; Harichandran and Vanmarcke, 1986; Shinozuka and Deodatis, 1991; Vanmarcke and Fenton, 1991), and became popular in the analyses of the multi-support structural response based on the random vibration approach. In the papers by Harichandran and Wang (1988, 1990), Zerva (1991), and Hao (1989, 1991), specific multi-support structures were analyzed, taking into account one- or two-dimensional random field models and the orientation of the structure with respect to the source direction (Zembaty, 1997) or local site effects (Zembaty and Rutenberg, 1998). Most of these analyses (except for very few, e.g., Perotti (1990)) assume stationarity of random vibrations. However, such an assumption may be disputable for some important multi-support structures like large bridges with fundamental periods of several seconds or more. On the other hand, there are methods available now (e.g., Gupta and Trifunac, 1998) that properly account for the nonstationarity of seismic excitation and response within the framework of stationary random vibrations.

The random vibration-based approach utilizing SMART-1 data provided good and general results on the spatial seismic effects on structures. However, in the inevitable temporal averaging of the multiple records from dense arrays of instruments, some important pieces of information can be lost, particularly those regarding the phasing and contributions of the specific wave types in the ground motion. Thus, an alternative approach to investigating the effects of the spatial nature of strong ground motion is deterministic and includes analyses of particular wave types arriving at the structures (Trifunac, 1997; Trifunac and Todorovska, 1997; Trifunac and Gicev, 2006) and their propagation inside the structures (Todorovska and Lee, 1989; Todorovska and Trifunac, 1989, 1990a).

The spatial seismic effects were also analyzed for extended structures like dams (Kojic and Trifunac, 1991a, 1991b), dikes (Todorovska et al., 2001a, 2001b), and selected lifeline structures (e.g., buried pipelines (Hindy and Novak, 1980; Datta, 1999). In this case, instead of differential motion among structural supports, continuous changes of the ground motion occur along the structure. Review of these problems is beyond the scope of this paper, but readers interested in this subject can find further examples in the papers by Novak (1990), Todorovska and Trifunac (1990b), Zerva and Shinozuka (1991), and Datta (1999), among others.

Since most of the analyses of spatial seismic effects on structures are strongly case-dependent, the generalizations of the response spectra to include the spatial effects were searched for, starting from the early proposals of Loh et al. (1982) and Abrahamson and Bolt (1985). Later, the concept of spatial response spectrum was further advanced to include its stochastic description (Zembaty and Krenk, 1993; Zembaty, 1996; Zembaty and Rutenberg, 2002). In a separate development, Der Kiureghian and Neuenhofer (1992) also proposed a concept of random vibration-based response spectrum method for MDOF systems under multi-support excitations, generalized from the earlier concepts of the response spectrum method for stationary random vibrations (Der Kiureghian, 1980, 1981).

In what follows, selected results from the analyses of the simplest SDOF stochastic spatial response spectra from Zembaty and Krenk (1993), Zembaty (1996), and Zembaty and Rutenberg (2002) will be reviewed. Some results of the column response spectra concept of Trifunac and Todorovska (1997), and Trifunac and Gicev (2006) will also be considered. These two approaches were chosen for this review because they cover, in the simplest possible way, most of the physically important aspects of structural response under spatial seismic excitations, and because, in a sense, they complement one another. Our review starts with the presentation of a stochastic model of spatial seismic excitations.

A COMPOSITE COHERENCY MODEL OF SPATIAL SEISMIC EFFECTS

Consider two points A and B on the ground surface. A convenient stochastic measure of the difference between the seismic signals at these two points is its complex coherency $\gamma_{AB}(\omega)$:

$$\gamma_{AB}(\omega) = |\gamma_{AB}|\exp[i\Theta_{AB}] = \frac{S_{AB}(\omega)}{\sqrt{S_A(\omega)S_B(\omega)}} \tag{1}$$

in which $S_A(\omega)$ and $S_B(\omega)$ stand for power spectral densities of accelerations measured along the same direction (*x*, *y*, or *z*) at points A and B, respectively; $|\gamma_{AB}|$ stands for the modulus of the coherence function; Θ_{AB} is the phase of the coherence function; and $S_{AB}(\omega)$ represents the co-spectrum of the two signals. The modulus of coherency $|\gamma_{AB}(\omega)|$ is called loss of coherency or lagged coherency. It is a measure of the similarity of signals at point A and B, excluding the effect of traveling waves, which is included in the phase Θ_{AB}. Sometimes the real value of coherency, $\mathrm{Re}(\gamma_{AB}(\omega))$, called the unlagged coherency, is analyzed. Equation (1) can be rewritten as

$$S_{AB}(\omega) = \gamma_{AB}(\omega)\sqrt{S_A(\omega)S_B(\omega)} \tag{2}$$

to display the dependence between the input spectral densities, S_A and S_B, their coherence γ_{AB}, and the output cross-spectral density function S_{AB}.

Der Kiureghian (1996) proposed a composite model of spatial seismic effects in which the cross-spectral density of accelerations was

$$\gamma_{AB}(\omega) = \gamma_{AB}^{(i)}(\omega)\gamma_{AB}^{(w)}(\omega)\gamma_{AB}^{(s)}(\omega) = \gamma_{AB}^{(i)}(\omega)\exp\left[i\left(\Theta_{AB}^{(w)}(\omega) + \Theta_{AB}^{(s)}(\omega)\right)\right] \tag{3}$$

This is composed of three principal factors, each representing a contribution from a different spatial seismic influence: $\gamma_{AB}^{(i)}$ is a measure of the loss of coherency between A and B; $\gamma_{AB}^{(w)}$ stands for complex coherency resulting from phase delay due to the wave propagation; and $\gamma_{AB}^{(s)}$ represents local site effects, where $i = \sqrt{(-1)}$. It should be pointed out that the loss of coherency is represented by a real function, whereas wave-passage and site effects result in the phase changes $\Theta_{AB}^{(w)}$ and $\Theta_{AB}^{(s)}$ of the complex coherency.

The complex coherency contains the key information on spatial distribution of seismic ground motions and constitutes the main input function for random vibration analyses of structural systems. Usually, its parameters are retrieved from the synchronized records of a particular seismic event (see, e.g., SMART-1 data processed by Hao (1989)). Two problems will be noted when analyzing physical interpretations of complex coherency:

- The modulus of coherency appears to be very sensitive to spatial separation, even for relatively low frequencies (Der Kiureghian and Neuenhofer, 1992). On the other hand, there is experimental evidence that during strong earthquakes the peak values of ground motion do not change substantially over rather long distances (Todorovska and Trifunac, 1997). Thus, direct observations of the moduli of coherency can be misleading about important peak response measures of the seismic ground motion.
- The second problem regarding the complex coherency concerns its phase. Usually, a single apparent wave velocity is assumed to describe the spatial phase changes of the coherency function, which is in direct violation of the observations of the records of real earthquakes.

Thus, deeper research regarding rational stochastic models of spatial seismic ground motion seems necessary and inevitable.

SPATIAL RESPONSE SPECTRUM FOR SDOF SYSTEM UNDER TWO-COMPONENT, RANDOM SEISMIC EXCITATIONS

Consider a simple oscillator under two different support excitations (Figure 2). Such a system, though very simple, can represent several important structural response cases, e.g., a symmetric beam vibrating in one dynamic mode (transverse, vertical, or axial; see Figure 3). Its equation of motion takes the form

$$\begin{bmatrix} m & 0 & 0 \\ 0 & 0 & 0 \\ 0 & 0 & 0 \end{bmatrix} \begin{bmatrix} \ddot{q}^t \\ \ddot{u}_A \\ \ddot{u}_B \end{bmatrix} + \begin{bmatrix} c & -c/2 & -c/2 \\ -c/2 & c/2 & 0 \\ -c/2 & 0 & c/2 \end{bmatrix} \begin{bmatrix} \dot{q}^t \\ \dot{u}_A \\ \dot{u}_B \end{bmatrix} + \begin{bmatrix} k & -k/2 & -k/2 \\ -k/2 & k/2 & 0 \\ -k/2 & 0 & k/2 \end{bmatrix} \begin{bmatrix} q^t \\ u_A \\ u_B \end{bmatrix} = \begin{bmatrix} 0 \\ 0 \\ 0 \end{bmatrix} \tag{4}$$

where q^t and q represent total and relative oscillator displacements, respectively (Figure 2). Introducing natural frequency $\omega_0 = \sqrt{(k/m)}$ and damping ratio $\xi = c/(2m\omega_0)$, after some algebra, the above equation can be reduced to that for a SDOF system:

$$\ddot{q} + 2\xi\omega_0\dot{q} + \omega_0^2 q = -\frac{1}{2}\left(\ddot{u}_A + \ddot{u}_B\right) \tag{5}$$

The column shear forces $f_A(t)$ and $f_B(t)$ are

$$f_A(t) = \frac{k}{2}\left(q^t - u_A\right) = \frac{k}{2}\left(\frac{u_B(t)}{2} - \frac{u_A(t)}{2} + q(t)\right) \tag{6a}$$

$$f_B(t) = \frac{k}{2}\left(q^t - u_B\right) = \frac{k}{2}\left(\frac{u_A(t)}{2} - \frac{u_B(t)}{2} + q(t)\right) \tag{6b}$$
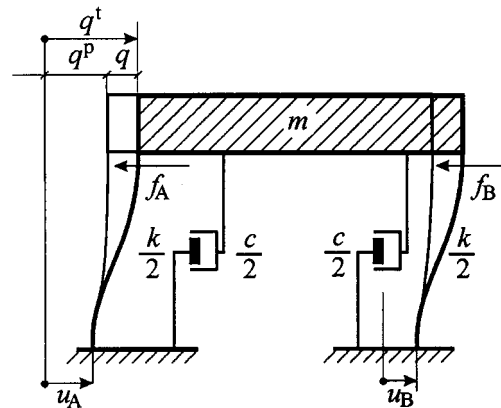

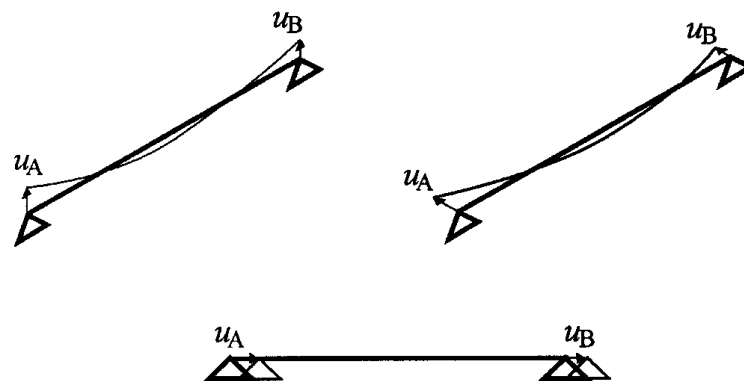Fig. 2 A single-degree-of-freedom system excited by two different motions

Fig. 3 Examples of simple structures that can be modeled by the SDOF system shown in Figure 2 (after Zembaty and Rutenberg, 2002)

Equation (5) expresses the simple fact that the dynamic response of the analyzed SDOF system represents an oscillator response to the average of support excitations u_A and u_B. Unlike the relative displacements $q(t)$, the force responses (Equations (6a) and (6b)) combine both the dynamic response

and pseudo-static vibrations. Therefore, they are more influenced by the asynchronous support motions than by the displacements of the oscillator.

We assume next that the excitations $u_A(t)$ and $u_B(t)$ can be presented by spectral Stieltjes-Fourier decomposition of stationary random processes:

$$u_A(t) = \int_{-\infty}^{\infty} e^{i\omega t} \mathrm{d}\hat{u}_A(\omega) \tag{7a}$$

$$u_B(t) = \int_{-\infty}^{\infty} e^{i\omega t} \mathrm{d}\hat{u}_B(\omega) \tag{7b}$$

in which $\hat{u}_A(\omega)$ and $\hat{u}_B(\omega)$ stand for random processes in the frequency domain with orthogonal increments:

$$< \mathrm{d}\hat{u}_A(\omega_1) \mathrm{d}\hat{u}_B^*(\omega_2) > = \begin{cases} S_{u_A u_B}(\omega)\mathrm{d}\omega & \text{for } \omega_1 = \omega_2 = \omega \\ 0 & \text{for } \omega_1 \neq \omega_2 \end{cases} \tag{8}$$

Here the symbol $< >$ denotes the mathematical expectation, asterisk stands for complex conjugate, and $S_{u_A u_B}(\omega)$ is the cross power spectral density of random processes $u_A(t)$ and $u_B(t)$. It should be noted that for stationary processes, $S_{u_A u_B}(\omega) = S_{\ddot{u}_A \ddot{u}_B}(\omega)/\omega^4$, and for brevity, the acceleration cross spectrum will be denoted by $S_{AB}(\omega)$ and the displacement cross spectra will be denoted by $S_{u_A u_B}(\omega)$. When the processes $u_A(t)$ and $u_B(t)$ are identical, the cross-spectral density in Equation (8) reduces to the respective auto-spectra $S_{u_A}(\omega) = S_{u_B}(\omega) = S_u(\omega)$. The solution of Equation (5) can be given in the form of Duhamel integral:

$$q(t) = -\frac{1}{2}\int_0^t h(\tau)\ddot{u}_A(t-\tau)\mathrm{d}\tau - \frac{1}{2}\int_0^t h(\tau)\ddot{u}_B(t-\tau)\mathrm{d}\tau \tag{9}$$

Transforming the above equation into the frequency domain, assuming stationarity, and substituting respective spectral representations (as in Equations (7a) and (7b)) for both displacements and accelerations leads to the following solution of Equation (5):

$$q(t) = -\frac{1}{2}\int_{-\infty}^{\infty} H(\omega)e^{i\omega t}\mathrm{d}\hat{\ddot{u}}_A(\omega) - \frac{1}{2}\int_{-\infty}^{\infty} H(\omega)e^{i\omega t}\mathrm{d}\hat{\ddot{u}}_B(\omega) \tag{10}$$

where $H(\omega) = (\omega_0^2 - \omega^2 + 2i\xi\omega_0\omega)^{-1}$ is the frequency response function of the oscillator. Analogous solutions for the forces f_A and f_B are

$$f_A(t) = \frac{k}{4}\left(\int_{-\infty}^{\infty} e^{i\omega t}\mathrm{d}\hat{u}_B(\omega) - \int_{-\infty}^{\infty} e^{i\omega t}\mathrm{d}\hat{u}_A(\omega) - \int_{-\infty}^{\infty} H(\omega)e^{i\omega t}\mathrm{d}\hat{\ddot{u}}_A(\omega) - \int_{-\infty}^{\infty} H(\omega)e^{i\omega t}\mathrm{d}\hat{\ddot{u}}_B(\omega) \right) \tag{11a}$$

$$f_B(t) = \frac{k}{4}\left(\int_{-\infty}^{\infty} e^{i\omega t}\mathrm{d}\hat{u}_A(\omega) - \int_{-\infty}^{\infty} e^{i\omega t}\mathrm{d}\hat{u}_B(\omega) - \int_{-\infty}^{\infty} H(\omega)e^{i\omega t}\mathrm{d}\hat{\ddot{u}}_A(\omega) - \int_{-\infty}^{\infty} H(\omega)e^{i\omega t}\mathrm{d}\hat{\ddot{u}}_B(\omega) \right) \tag{11b}$$

Taking into account that $S_{\ddot{u}}(\omega) = \omega^2 S_{\dot{u}}(\omega) = \omega^4 S_u(\omega)$, and introducing the complex coherency $\gamma_{AB}(\omega)$ for signals $\ddot{u}_A(t)$ and $\ddot{u}_B(t)$ (in the format of Equation (1)), we can formulate the following spectral matrix for the vector, $[u_A(t) \quad u_B(t) \quad \ddot{u}_A(t) \quad \ddot{u}_B(t)]^T$, which will be useful in deriving formulas for the spectral densities of displacements and forces in the next two points,

$$
\begin{bmatrix}
\dfrac{1}{\omega^4} S_A & \dfrac{1}{\omega^4}\gamma_{AB}\sqrt{S_A S_B} & -\dfrac{1}{\omega^2} S_A & -\dfrac{1}{\omega^2}\gamma_{AB}\sqrt{S_A S_B} \\[2ex]
\dfrac{1}{\omega^4}\gamma_{AB}^{*}\sqrt{S_A S_B} & \dfrac{1}{\omega^4} S_B & -\dfrac{1}{\omega^2}\gamma_{AB}^{*}\sqrt{S_A S_B} & -\dfrac{1}{\omega^2} S_B \\[2ex]
-\dfrac{1}{\omega^2} S_A & -\dfrac{1}{\omega^2}\gamma_{AB}\sqrt{S_A S_B} & S_A & \gamma_{AB}\sqrt{S_A S_B} \\[2ex]
-\dfrac{1}{\omega^2}\gamma_{AB}^{*}\sqrt{S_A S_B} & -\dfrac{1}{\omega^2} S_B & \gamma_{AB}^{*}\sqrt{S_A S_B} & S_B
\end{bmatrix}
\tag{12}
$$

The symbols $S_A \equiv S_A(\omega)$, $S_B \equiv S_B(\omega)$ denote (real) point spectral densities of the accelerations $\ddot{u}_A(t)$ and $\ddot{u}_B(t)$. Further analysis depends upon the type of spatial seismic effects to be analyzed (see Equation (3)).

1. The Effect of Wave Passage and Loss of Coherency on Response Spectra

We first assume that both supports A and B have exactly the same site conditions and are separated by the distance $d = |AB|$. In this case, both input spectral densities of accelerations are identical, $S_{\ddot{u}_A}(\omega) = S_{\ddot{u}_B}(\omega)$, and are denoted here for brevity by $S(\omega)$. Following Equation (2), their cross-spectral density equals

$$
S_{AB}(\omega) = \gamma_{AB}(\omega) S(\omega)
\tag{13}
$$

The matrix in (12) can then be simplified to

$$
\begin{bmatrix}
\dfrac{1}{\omega^4} & \dfrac{1}{\omega^4}\gamma_{AB}(\omega) & -\dfrac{1}{\omega^2} & -\dfrac{1}{\omega^2}\gamma_{AB}(\omega) \\[2ex]
\dfrac{1}{\omega^4}\gamma_{AB}^{*}(\omega) & \dfrac{1}{\omega^4} & -\dfrac{1}{\omega^2}\gamma_{AB}^{*}(\omega) & -\dfrac{1}{\omega^2} \\[2ex]
-\dfrac{1}{\omega^2} & -\dfrac{1}{\omega^2}\gamma_{AB}(\omega) & 1 & \gamma_{AB}(\omega) \\[2ex]
-\dfrac{1}{\omega^2}\gamma_{AB}^{*}(\omega) & -\dfrac{1}{\omega^2} & \gamma_{AB}^{*}(\omega) & 1
\end{bmatrix} S(\omega)
\tag{14}
$$

Since only the loss of coherence and wave passage effects are analyzed, following Equation (3), it follows that

$$
S_{AB}(\omega) = \left| \gamma_{AB}^{(i)}(\omega) \right| \exp\left[i\Theta_{AB}^{(w)}(\omega) \right] S(\omega)
\tag{15}
$$

The loss of coherency denoted here as $|\gamma_{AB}^{(i)}|$ is a real function of frequency ω and distance d, decreasing from 1 at $d = 0$ to 0 for $d \to \infty$. A simple form of the loss of coherency was proposed by Luco and Wong (1986):

$$
\left| \gamma_{AB}^{(i)}(\omega) \right| = \exp\left[-(\kappa d \omega)^2 \right]
\tag{16}
$$

where κ is a real parameter that controls the dependence of the loss of coherency to remain between 0 and 1.

The auto-spectrum of accelerations $S(\omega)$ often applied in engineering random vibration analyses consists of the familiar Kanai-Tajimi spectral density (Kanai, 1957; Tajimi, 1960) with a filter proposed later by Ruiz and Penzien (1969). Its detailed form is given in Appendix A.

Assuming the plane waves to be propagating with the same apparent velocity, v_g, for all frequencies, the phase term in Equation (15) becomes

$$
\Theta_{AB}^{(w)}(\omega) = \frac{\omega d}{v_g}
\tag{17}
$$

Taking into account Equations (10)–(11) and 14, we can write the equations for spectral densities of relative displacements:

$$S_q(\omega, \omega_0) = \frac{1}{2} |H(\omega, \omega_0)|^2 \left[1 + \text{Re}\left(\gamma_{AB}(\omega)\right)\right] S(\omega) \tag{18}$$

and for column shear forces:

$$S_{f_A}(\omega, \omega_0) = \frac{k^2}{8} \left(\frac{1}{\omega^4} \left[1 - \text{Re}\left(\gamma_{AB}(\omega)\right)\right] - \frac{1}{\omega^2} \text{Im}\left(H(\omega, \omega_0)\right) \text{Im}\left(\gamma_{AB}(\omega)\right)\right.$$
$$\left. + |H(\omega, \omega_0)|^2 \left[1 + \text{Re}\left(\gamma_{AB}(\omega)\right)\right]\right) S(\omega) \tag{19a}$$

$$S_{f_B}(\omega, \omega_0) = \frac{k^2}{8} \left(\frac{1}{\omega^4} \left[1 - \text{Re}\left(\gamma_{AB}(\omega)\right)\right] + \frac{1}{\omega^2} \text{Im}\left(H(\omega, \omega_0)\right) \text{Im}\left(\gamma_{AB}(\omega)\right)\right.$$
$$\left. + |H(\omega, \omega_0)|^2 \left[1 + \text{Re}\left(\gamma_{AB}(\omega)\right)\right]\right) S(\omega) \tag{19b}$$

The above force spectral densities consist of three terms reflecting (a) the pseudo-static dynamic contribution, (b) cross pseudo-static-dynamic contribution, and (c) the dynamic contribution, respectively. It is noted that the sign of the second term depends upon the wave direction (from *A* to *B* or vice-versa). However, as shown by Zembaty (1996), the contribution of the second term does not exceed a few percent for the realistic values of excitation parameters. Thus, the force spectrum can be approximated by a formula that does not depend upon the direction of wave propagation:

$$S_f(\omega, \omega_0) \cong \frac{k^2}{8} \left(\frac{1}{\omega^4} \left[1 - \text{Re}\left(\gamma_{AB}(\omega)\right)\right] + |H(\omega, \omega_0)|^2 \left[1 + \text{Re}\left(\gamma_{AB}(\omega)\right)\right]\right) S(\omega) \tag{20}$$

In Figure 4, this force spectral density is shown as a function of separation distance *d* for structural damping ratio $\xi = 0.05$ and $v = 1000$ m/s. It can be seen from this figure how the pseudo-static contribution in the response (the second "hill" close to the resonance peak) increases with the increasing separation distance.
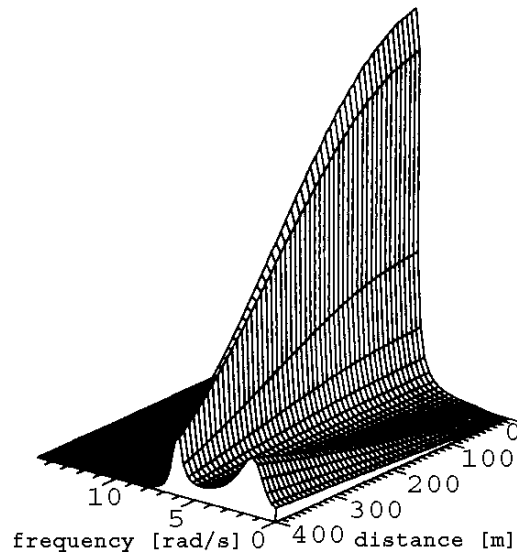

Fig. 4   Spectral density of force response versus frequency and separation distance $d = |AB|$ for $\omega_0 = 2\pi$ rad/s, structural damping ratio $\xi = 0.05$, and apparent wave velocity $v = 1000$ m/s (after Zembaty and Krenk, 1993)

Integrating the preceding spectral densities with respect to ω for various values of natural frequency ω_0, we obtain the displacement mean-square response spectrum:

$$\sigma_q^2(\omega_0) = \int_{-\infty}^{\infty} S_q(\omega,\omega_0)\mathrm{d}\omega \tag{21}$$

and the force mean-square response spectrum:

$$\sigma_f^2(\omega_0) = \int_{-\infty}^{\infty} S_f(\omega,\omega_0)\mathrm{d}\omega \tag{22}$$

In Figure 5, the force root-mean-square (RMS) response spectrum is shown for $v_g = 1000$ m/s and five values of separation distance d from zero to 400 m. When $d = 0$ (see the dashed line), the force response spectrum goes to zero with decreasing natural period, as it does for a typical displacement response spectrum. This is so because, for the uniform excitations, the force response is a direct function of relative displacement q. It is interesting to note how, for spatial excitations, the force response spectrum goes to a finite, constant value reflecting the purely pseudo-static oscillator response for longer support distances.
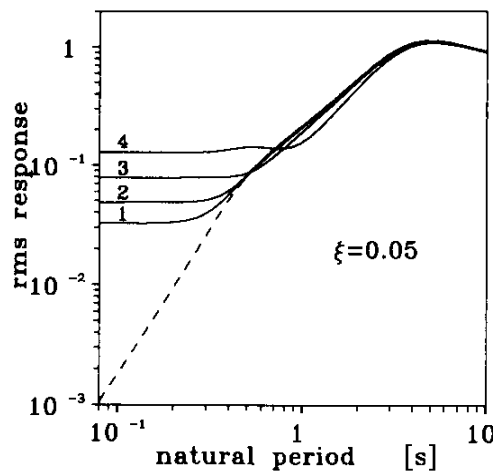

Fig. 5   RMS response spectrum for separation distance $d = 0$ (dashed line) and $d = 50, 100, 200, 400$ m (solid lines, '1', '2', '3' and '4', respectively) (after Zembaty and Krenk, 1993)

The RMS response spectra can be normalized with respect to coherent excitations $(d = 0)$. This leads to the following displacement and force response ratios:

$$\Phi_q(\omega_0) = \frac{\sigma_q(\omega_0)}{\sigma_q^{\text{coher}}(\omega_0)} \tag{23}$$

$$\Phi_f(\omega_0) = \frac{\sigma_f(\omega_0)}{\sigma_f^{\text{coher}}(\omega_0)} \tag{24}$$

It can be seen that the response spectra are controlled by three parameters: loss of coherency $|\gamma_{AB}(\omega)|$ measured by the parameter κ, support distance d, and the velocity of wave propagation v_g. To make the analysis more clear, a reduced velocity, $v_r = v_g / d$, and a parameter of reduced loss of coherency, $\kappa_r = \kappa d$, are introduced now. The reduced velocity measures the apparent wave velocity in terms of support distance d, while κ_r is a measure of the actual loss of coherency. With these changes, the equation for complex coherency takes the following form:

$$\gamma_{AB}(\omega,\kappa_r,v_r) = \exp\left[-(\kappa_r\omega)^2\right]\exp\left[i\omega/v_r\right] \tag{25}$$

Substituting for the complex coherency in Equations (18) and (20), its exponential form (Equation (25)), and applying Euler's formula gives the following results for displacement and force spectral densities:

$$S_q\left(\omega,\omega_0,\kappa_r,v_r\right)=\frac{1}{2}\left|H(\omega,\omega_0)\right|^2\left[1+\left|\gamma_{AB}\left(\omega,\kappa_r\right)\right|\cos\left(\omega/v_r\right)\right]S(\omega) \qquad (26)$$

$$S_f(\omega,\omega_0,\kappa_r,v_r)=$$

$$\frac{k^2}{8}\left(\frac{1}{\omega^4}\left[1-|\gamma_{AB}(\omega,\kappa_r)|\cos(\omega/v_r)\right]+\left|H(\omega,\omega_0)\right|^2\left[1+|\gamma_{AB}(\omega)|\cos(\omega/v_r)\right]\right)S(\omega) \qquad (27)$$

We illustrate the effects of κ_r and v_r on the displacement (see Figure 6) and force response ratio (see Figure 7) for natural period $T_0 = 1$ s ($\omega_0 = 2\pi$ rad/s). The displacement spectrum always stays below 1, expressing the fact that the combined displacements represent the averaging effect of both support excitations. On the other hand, the force ratio stays either below 1 or above 1, mostly when the velocity is low or κ_r is high (i.e., faster loss of coherency). The values of Φ_f greater than 1 indicate a non-conservative result of spatial seismic effects, occurring mostly in situations when the pseudo-static effects dominate the structural vibrations. It can be seen from Figure 7 that the effect of parameter κ_r on the force response ratio is more important for higher velocities than for the lower ones.
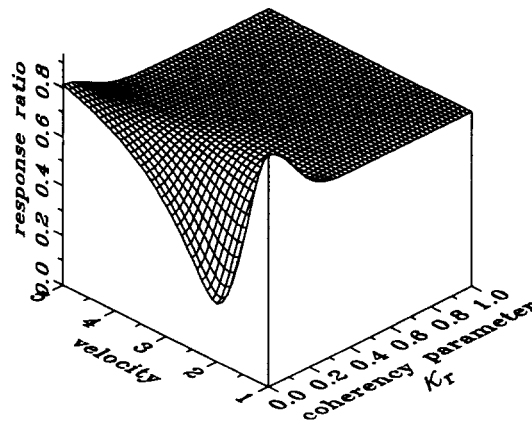

Fig. 6   Effect of loss of coherency κ_r and reduced velocity v_r on the displacement response ratio for $\omega_0 = 2\pi$ rad/s and $\xi = 0.05$ (after Zembaty, 1996)
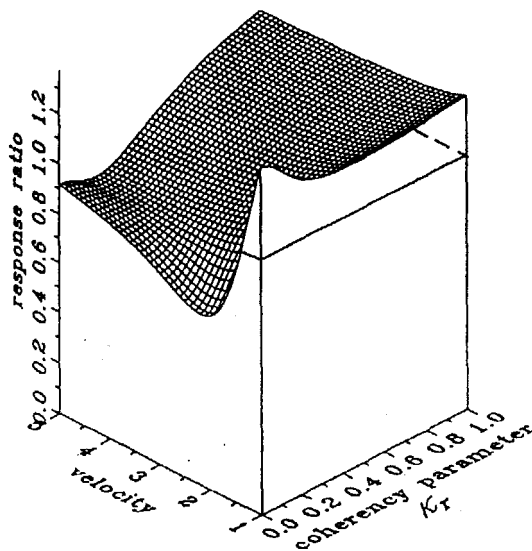

Fig. 7   Effect of loss of coherency κ_r and reduced velocity v_r on the force response ratio for $\omega_0 = 2\pi$ rad/s and $\xi = 0.05$ (after Zembaty, 1996)

Next, consider various limits of coefficients Φ_q and Φ_f (see Equations (23) and (24)). When $|\gamma_{AB}|$ goes to 1 (or κ_r goes to 0), there is no loss of coherency for the excitations at points A and B (e.g., for short support distance or no wave attenuation), and only the wave passage contributes to the spatial effects. Equations (26) and (27) then simplify to

$$S_q(\omega, \omega_0, \kappa_r, v_r) = \frac{1}{2}|H(\omega, \omega_0)|^2 \left[1 + \cos(\omega/v_r)\right] S(\omega) \tag{28}$$

$$S_f(\omega, \omega_0, \kappa_r, v_r) = \frac{k^2}{8}\left(\frac{1}{\omega^4}\left[1 - \cos(\omega/v_r)\right] + |H(\omega, \omega_0)|^2 \left[1 + \cos(\omega/v_r)\right]\right) S(\omega) \tag{29}$$

The displacement response ratio (see Equations (23) and (28)) and the force response ratio (see Equations (24) and (29)) are shown in Figures 8 and 9, respectively, as the functions of natural frequency and velocity for v_r varying from 1 to 5. The displacement ratio is always less than 1 and oscillates rapidly with both natural frequency and velocity. On the other hand, the force ratio can be either less or greater than 1, depending upon the natural frequency and velocity. For a low natural frequency, the force ratio increases with increasing velocity and approaches 1. For a higher natural frequency the force ratio decreases with increasing velocity. This difference is based on the fact that for a higher natural frequency and lower velocity the pseudo-static motion dominates in the force response.
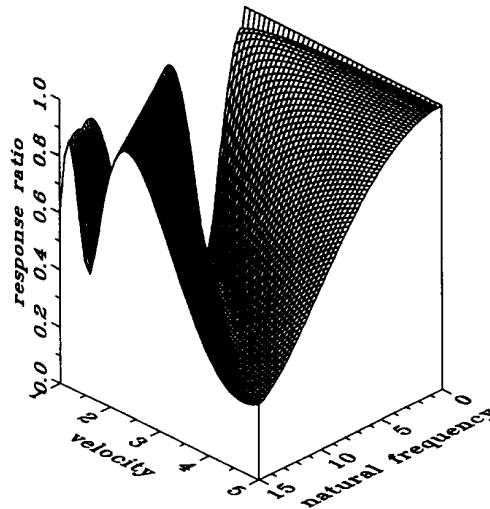

Fig. 8 Displacement response ratio (Equations (15) and (23)) versus reduced velocity v_r and natural frequency ω_0 (after Zembaty, 1996)
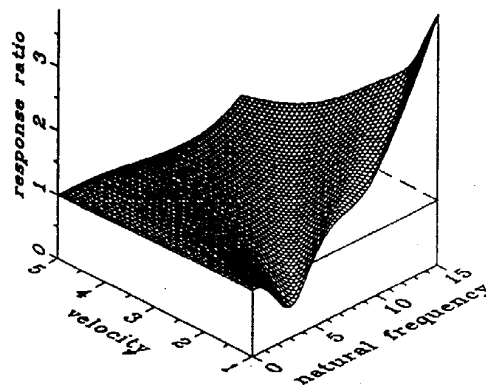

Fig. 9 Force response ratio (Equations (20) and (24)) versus reduced velocity v_r and natural frequency ω_0 (after Zembaty, 1996)

Consider now a situation in which $|\gamma_{AB}|$ goes to 0 (or κ_r goes to infinity):

$$S_q(\omega, \omega_0, \kappa_r, v_r) = \frac{1}{2}|H(\omega, \omega_0)|^2 S(\omega) \qquad (30)$$

$$S_f(\omega, \omega_0, \kappa_r, v_r) = \frac{k^2}{8}\left(\frac{1}{\omega^4} + |H(\omega, \omega_0)|^2\right)S(\omega) \qquad (31)$$

In this case there is a total loss of coherency between support points, regardless of the distance or wave velocity. The oscillating cosine terms (from wave propagation) vanish. The displacement spectral density equals just half of the solution for uniform excitations. The force spectral density displays two terms contributing to both the pseudo-static and dynamic motions.

Next, we consider the limits of Equations (26) and (27) when the reduced velocity v_r goes to infinity. The spectral densities depend now only upon the loss of coherency, and again the oscillating terms vanish:

$$S_q(\omega, \omega_0, \kappa_r, v_r) = \frac{1}{2}|H(\omega, \omega_0)|^2\left[1 + |\gamma_{AB}(\omega, \kappa_r)|\right]S(\omega) \qquad (32)$$

$$S_f(\omega, \omega_0, \kappa_r, v_r) = \frac{k^2}{8}\left(\frac{1}{\omega^4}[1 - |\gamma_{AB}(\omega, \kappa_r)|] + |H(\omega, \omega_0)|^2[1 + |\gamma_{AB}(\omega)|]\right)S(\omega) \qquad (33)$$

If v_r goes to 0, formulas as in Equations (26) and (27) diverge and the outcome cannot be predicted.

2. Spatial Response Spectra and Local Site Effects

We consider next a situation depicted schematically in Figure 10. The simple two-support oscillator shown in Figure 2 is now supported with its left column (*A*) on a rock outcrop, while its right column (*B*) is on a soil layer overlaying the bedrock. Such a situation may easily happen for folded sedimentary rocks exposed at the surface or in the basins generated by the folding of sedimentary rocks in alluvial river valleys. In such cases, the significant lateral heterogeneity may be observed even for the adjacent sites, for which the wave passage effects and loss of coherency effects may be less important. For this reason, and to make further analysis more clear, it is assumed now that only site effects are considered and that there is "neither loss of coherency nor wave passage between the sites *A* and *B*" (the "bedrock" motion $x(t)$ in Figure 10 is assumed to be identical for the two sites). The site effects are modeled by the local soil frequency response functions $H_A(\omega)$ and $H_B(\omega)$ at the two stations. This leads to the following relation between the bedrock acceleration cross-spectral density $S_{AB}^{(b)}(\omega)$ and the surface acceleration cross-spectral density $S_{AB}^{(r)}(\omega)$:

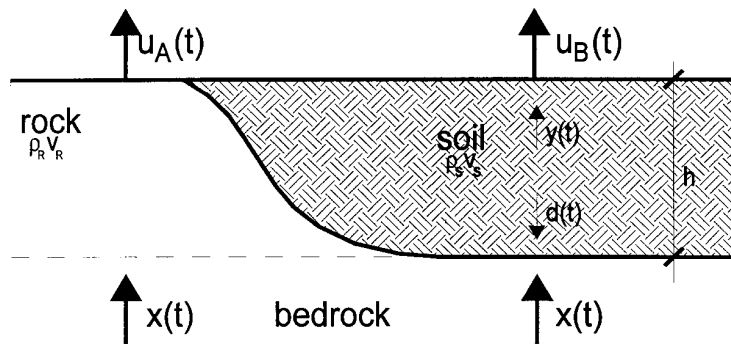$$S_{AB}^{(r)}(\omega) = H_A(\omega)H_B^* S_{AB}^{(b)}(\omega) \qquad (34)$$

Fig. 10 Ground motion from bedrock to the surface for rock outcrop (left) and for a soil layer (right) (after Zembaty and Rutenberg, 2002)

When the two sites A and B coincide, these cross-spectra reduce to the respective auto-spectra, and instead of Equation (34) we can write two equations for the sites *A* and *B*:

$$S_{AA}^{(r)}(\omega) = \left| H_A(\omega) \right|^2 S_{AA}^{(b)}(\omega) \tag{35a}$$

$$S_{BB}^{(r)}(\omega) = \left| H_B(\omega) \right|^2 S_{BB}^{(b)}(\omega) \tag{35b}$$

When only the site effects are considered, as is the case for this point, the complex coherency γ_{AB} includes only the third term of Equation (3):

$$\gamma_{AB}(\omega) = \gamma_{AB}^{(s)}(\omega) = \exp\left[i\Theta_{AB}^{(s)}(\omega) \right] \tag{36}$$

with the phase difference $\Theta_{AB}^{(s)}(\omega)$ given by

$$\Theta_{AB}^{(s)}(\omega) = \arctan \frac{\operatorname{Im}\left[H_A(\omega)H_B^*(\omega) \right]}{\operatorname{Re}\left[H_A(\omega)H_B^*(\omega) \right]} \tag{37}$$

Using Equations (10) and (11) and applying the orthogonality property (Equation (8)) together with the co-spectral matrix (Equation (12)), we can obtain the mean square displacements from

$$S_q(\omega, \omega_0) = \frac{1}{2}|H|^2 \left(\frac{|H_A|^2 + |H_B|^2}{2} + |H_A||H_B|\operatorname{Re}(\gamma_{AB}) \right) S \tag{38}$$

and forces from

$$S_{f_A}(\omega, \omega_0) = \frac{k^2}{8} \left\{ \frac{1}{\omega^4} \left[\frac{|H_A|^2 + |H_B|^2}{2} - |H_A||H_B|\operatorname{Re}(\gamma_{AB}) \right] \right.$$
$$- \frac{2}{\omega^2} \left(\frac{|H_A|^2 - |H_B|^2}{2} \operatorname{Re} H + |H_A||H_B|\operatorname{Im} H \operatorname{Im}(\gamma_{AB}) \right)$$
$$\left. + |H|^2 \left[\frac{|H_A|^2 + |H_B|^2}{2} + |H_A||H_B|\operatorname{Re}(\gamma_{AB}) \right] \right\} S \tag{39a}$$

$$S_{f_A}(\omega, \omega_0) = \frac{k^2}{8} \left\{ \frac{1}{\omega^4} \left[\frac{|H_A|^2 + |H_B|^2}{2} - |H_A||H_B|\operatorname{Re}(\gamma_{AB}) \right] \right.$$
$$- \frac{2}{\omega^2} \left(\frac{|H_A|^2 - |H_B|^2}{2} \operatorname{Re} H + |H_A||H_B|\operatorname{Im} H \operatorname{Im}(\gamma_{AB}) \right)$$
$$\left. + |H|^2 \left[\frac{|H_A|^2 + |H_B|^2}{2} + |H_A||H_B|\operatorname{Re}(\gamma_{AB}) \right] \right\} S \tag{39b}$$

in which the dependence on ω for the parameters on the right side of these equations is dropped for brevity. As before, the difference between forces f_A and f_B depends upon the sign of the second, cross-acceleration-displacement component. As will be shown later, the difference between these two forces may be substantial, particularly when the properties of the sites are drastically different. Integrating the spectral densities (Equations (38), (39a), and (39b)) with respect to ω leads to the RMS response

$$\sigma_{\text{resp}}^2(\omega_0) = \int_{-\infty}^{\infty} S_{\text{resp}}(\omega, \omega_0) d\omega \tag{40}$$

where subscript 'resp' represents either displacement q or force f_A or f_B. Normalization of the resulting RMS response may be done with respect to the RMS response at the soil site at one of the two points A or B or with respect to the rock properties at both sites. The latter normalization seems more appropriate in this case:

$$\Phi(\omega_0) = \frac{\sigma_{\text{resp}}(\omega_0)}{\sigma_{\text{resp}}^{\text{rock}}(\omega_0)} \tag{41}$$

Next, we present selected examples of the sensitivity analysis of the above spatial seismic coefficient for the SDOF system shown in Figure 2, when it is resting on a rock-soil system (see Figure 10). Adopting the soil model of Safak (1995), after some algebra (Zembaty and Rutenberg, 2002), transfer function of the soil layer is obtained as

$$H_S(\omega) = \frac{\left(1 + r - \dfrac{i}{4Q}\right) \exp\left[-i\omega\tau_S\left(1 - i/2Q\right)\right]}{1 + \left(r - \dfrac{i}{4Q}\right) \exp\left[-2i\omega\tau_S\left(1 - i/2Q\right)\right]} \tag{42}$$

in which τ_S is the S-wave propagation time in soil ($\tau_S = h/v_S$; see Figure 10), and Q is the quality factor measuring the ability of the medium to attenuate seismic waves. This can be related to the soil damping ratio as $\xi_{\text{soil}} = 1/(2Q)$. Finally, r is the wave-reflection coefficient:

$$r = \frac{\rho_R v_R - \rho_S v_S}{\rho_R v_R + \rho_S v_S} \tag{43}$$

for two media with mass densities, ρ_R and ρ_S, and S-wave velocities, v_R and v_S (here, these media are rock and soil, respectively). An analogous measure of the two media interfaces can be given by the rock/soil impedance ratio (e.g., Roesset, 1977):

$$I_{R/S} = \frac{\rho_R v_R}{\rho_S v_S} \tag{44}$$

In contrast to the soil transfer function $H_S(\omega)$, the transfer function of the rock outcrop represents only the propagation time in rock $\tau_R = h/v_R$ and equals

$$H_R(\omega) = \exp(-i\omega\tau_R) \tag{45}$$

Consider now the rock and soil parameters as follows: $\rho_R = 3$ g/cm³, $v_R = 1500$ m/s, $\rho_S = 2$ g/cm³, $v_S = 750$ m/s, $h = 150$ m, $Q = 30$. For these data, the reflection coefficient $r = 0.5$; propagation times in soil and rock are, respectively, $\tau_S = 0.2$ s, $\tau_R = 0.1$ s; and the first three soil "resonant" frequencies are 7.85, 23.6, and 39.3 rad/s (i.e., the peaks of transfer functions from Equations (39a) and (39b)). In Figure 11, the spectral density of displacements (as in Equation (38); see upper part of the figure) and forces f_A and f_B (as in Equations (39a) and (39b); see lower part of the figure) are plotted for the oscillator with $\omega_0 = 2$ rad/s ($T_0 = 1$ s). The displacement spectral density is that of a typical oscillator response to wide-band excitations, with most of the spectrum concentrated about the resonant frequency $\omega_0 = 2\pi$. On the other hand, in addition to the resonance peak, the force spectral densities display a low frequency "peak" resulting from the pseudo-static component of motion. The difference between the spectral densities of the forces f_A and f_B is very small for the above values of soil and oscillator parameters, and the presence of soil resonance cannot be seen in the displacement spectral density plots. Also, the second resonance of the forces at $\omega = 23.6$ rad/s can hardly be detected (see the lower part of Figure 11).

Next, consider the mean-square response. The RMS displacement response spectrum is shown in Figure 12(a) for the soil parameters, $\rho_S = 2$ g/cm³, $v_S = 750$ m/s, $Q = 30$, and soil depth $h = 150$ m. The same displacement response spectrum is shown again in Figure 12(b), after normalization with respect to Equation (41). The two plots in Figures 12(a) and 12(b) differ substantially. As would be expected, the RMS displacement response spectrum decreases steadily as T_0 goes to zero. In contrast, the normalized plot stays well below 1 for T_0 less than about 0.1 s, showing some excursions above 1 for $0.1 < T_0 < 1$, and it decays to 1 for $T_0 > 1$. The peaks of the plot in Figure 12(b) reflect the oscillator-soil resonance. As the natural period decreases, the peaks also decrease.
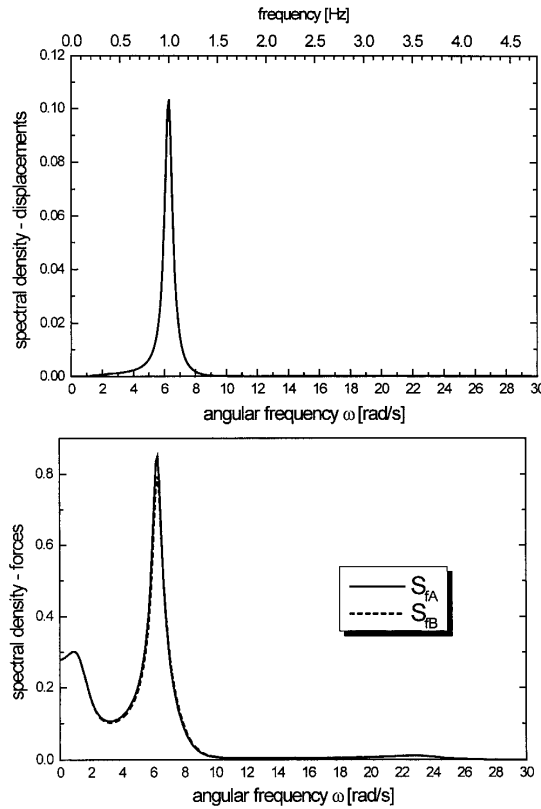
Fig. 11 SDOF system spectral densities (for $\omega_0 = 2\pi$ rad/s, $\xi = 0.05$, $\rho_R = 3$ g/cm^3, $v_R = 1500$ m/s, $\rho_S = 2$ g/cm^3, $v_S = 750$ m/s, $h = 150$ m, $Q = 30$, $r = 0.5$): displacements (upper) and forces f_A and f_B (lower) (after Zembaty and Rutenberg, 2002)
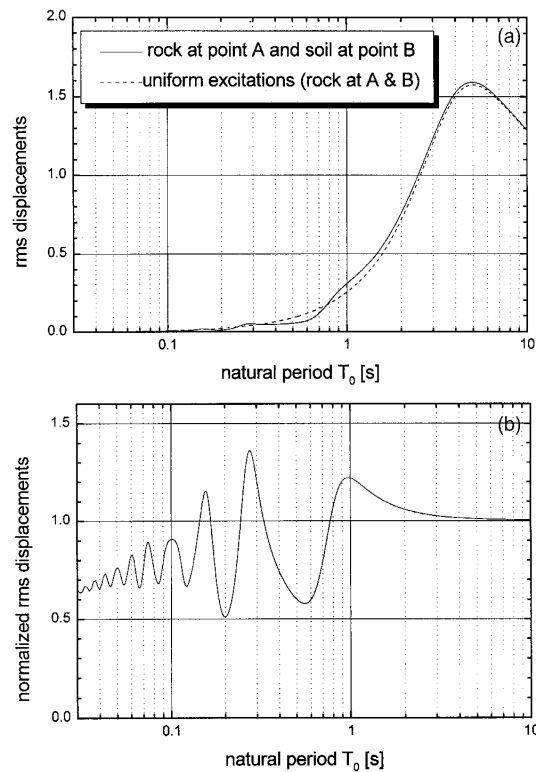

Fig. 12 RMS response spectra for (a) displacements, and (b) displacements normalized with respect to uniform excitations at A and B (rock at both sites) (after Zembaty and Rutenberg, 2002)

The plots of force response spectra (for forces f_A and f_B) are shown for the same set of parameters (ρ_S = 2 g/cm^3, v_S = 750 m/s, Q = 30) in Figure 13. Unlike the displacements, the force response spectra in Figure 13(a) do not vanish with falling T_0. This is due to the fact that as the inertial effects are reduced, the pseudo-static effects remain, and the response spectra stabilize at some level. In contrast, the force response spectra calculated for uniform excitations go down to zero (similarly as the displacements do) because in this case the pseudo-static effects do not induce forces, i.e., there is no differential motion between the two supports. Thus, the normalized RMS forces increase to infinity with vanishing natural period. Similar effects can be observed when considering the wave-passage effects for multi-support structures on uniform soil (Trifunac and Todorovska, 1997; Zembaty and Krenk, 1993; Zembaty, 1996). Obviously, the large values of the normalized response at very low natural periods shown in Figure 13(b) represent in some cases an "artificial" effect, as soil compliance can reduce it substantially.
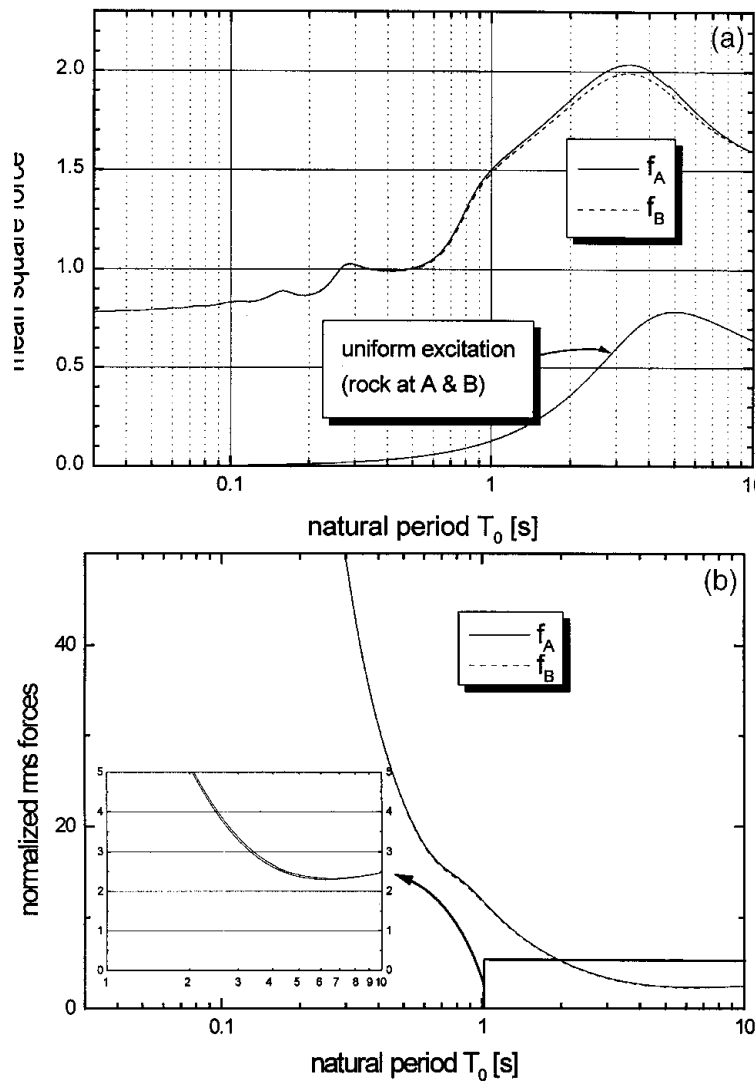

Fig. 13 (a) Spectra for forces f_A and f_B; (b) Force spectra normalized with respect to uniform excitations (rock at A and B) (after Zembaty and Rutenberg, 2002)

Finally, the ranges of the analyzed response spectra are illustrated in Figure 14 for v_S = 750 m/s and ρ_S varying from 2 to 3 g/cm^3 (see Figures 14(a) and 14(c)), as well as for v_S = 200 m/s and ρ_S = 1.5–2.5 g/cm^3 (see Figures 14(b) and 14(d)). These two values of v_S represent firm (soft) rock and very soft soils, respectively. The range of ρ_S represents variations in soil properties that are likely to be found in practice. The corresponding variations of the rock/soil impedance ratio range from 2 to 3 for v_S =

750 m/s, and from 9 to 15 for $v_S = 200$ m/s. As can be seen from the plots in Figures 14(a) –14(d), these variations of soil properties do not substantially affect the results for firm soil ($v_S = 750$ m/s). They do affect the displacements and force response spectra for soft soils ($v_S = 200$ m/s), but only for the first resonance peak at $T_0 \approx 3$ s. For the force response spectra and $v_S = 200$ m/s, a shift in the first resonance peaks of forces f_A and f_B can be observed. It can also be seen that the differences among shear forces f_A and f_B can be more pronounced even for quite realistic values of soil parameters.
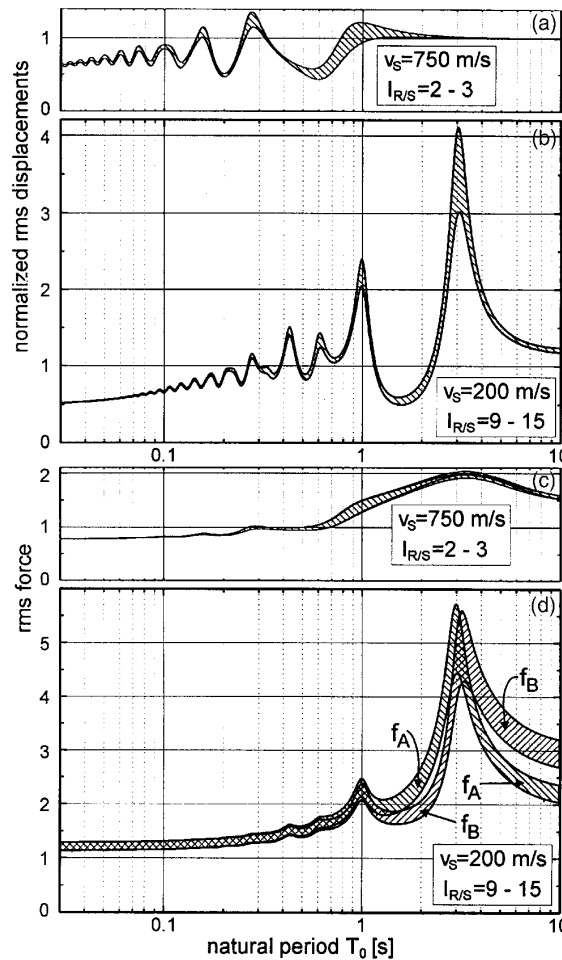

Fig. 14   Range of normalized displacement response spectra ((a), (b)) and force response spectra ((c), (d)) reflecting the range of soil densities $\rho_S = 1.5$–2.0 g/cm^3 for $v_S = 750$ m/s ($r = 0.333$–0.500, shear moduli $G_S = 1125$–1687 MPa, $I_{R/S} = 2$–3), and densities $\rho_S = 1.5$–2.0 g/cm^3 for $v_S = 200$ m/s ($r = 0.800$–0.875, $I_{R/S} = 9$–15) (after Zembaty and Rutenberg, 2002)

RESPONSE SPECTRA FOR COLUMN VIBRATIONS UNDER KINEMATIC WAVE EXCITATIONS

1. Response Spectra for In-plane Differential Motion of Columns of a Building Structure

Trifunac and Todorovska (1997) explored another approach to the problem of spatial seismic response spectra. They analyzed a multi-support, multi-column structure with a stiff first floor (see Figure 15). This structure is excited by the horizontal ground motions $u_1(t)$, $u_2(t)$,...,$u_n(t)$ and is situated along the radial direction of the wave propagation from the earthquake source (it is the most

conservative assumption in this case). Two types of waves may take part in these excitations: body waves incident with some angle γ, and surface (Rayleigh) waves. To simplify the analysis, the equivalent phase velocity c_{eq} was introduced, which is constant in time and frequency domain and represents all of the surface wave modes and the body waves propagating among the supports of the structure (Trifunac and Lee, 1996; Trifunac et al., 1996). Based on the detailed experimental data (Trifunac, 1971; Bycroft, 1983), it was possible to assume $c_{eq} \approx \beta_{av}$, where β_{av} is the average shear-wave velocity in the top 30 m below the ground surface. Next, a special reference point R on the ground surface was defined (see Figure 15), to which the individual support motion $u_i(t)$ was related. The point R was defined in such a way that its displacement $u_0(t)$ was a weighted average of the motions at the base of the columns:

$$u_0(t) = \frac{\sum_{i=1}^{n} k_i u_i(t)}{\sum_{i=1}^{n} k_i} \qquad (46)$$

By considering the strain field in the ground, together with limits for the possible wavelengths along the structure, and by making further detailed assumptions based on earlier experimental studies (Trifunac and Lee, 1996; Trifunac et al., 1996), Trifunac and Todorovska (1997) proposed quite a simple formulation of the response spectrum for differential motion of columns defined for the one-storey structure of Figure 15:

$$SDC(T, \xi, \tau) = \max_{t} \left[u^r(t) + v(t)\tau - \tfrac{1}{2} a(t)\tau^2 \right] \qquad (47)$$

Here, T stands for the natural period of the structure, ξ is the damping ratio, u^r denotes the relative displacements of the mass (with respect to the reference point R), $v(t)$ and $a(t)$ stand for the velocity and acceleration of the point R, and finally τ is the time required for a wave to propagate from the point R to the ith analyzed column. Assuming reasonable building dimensions and taking into account realistic, experimentally verified wavelengths the values of τ were suggested to stay between 0.001 and 0.1 s.
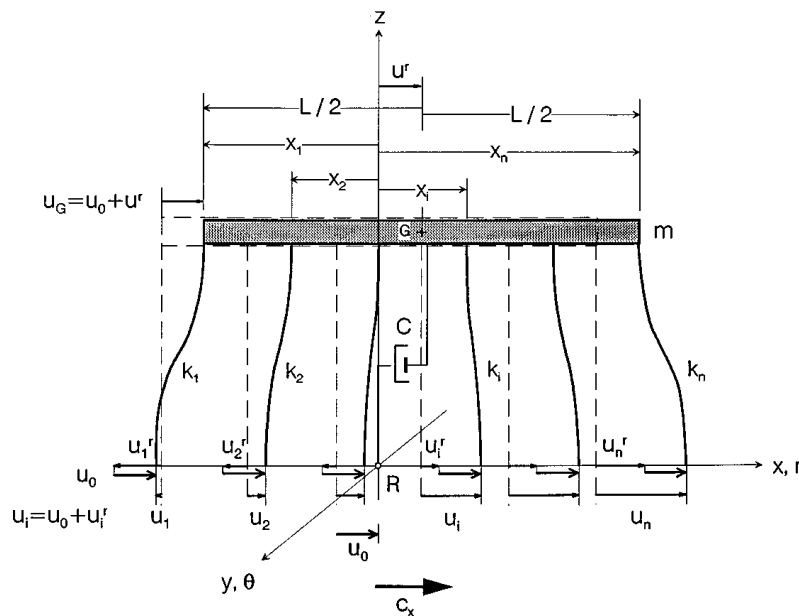

Fig. 15 Model of the one-storey structure excited by horizontal components of Rayleigh and/or SV waves (the columns have stiffness k_i; absolute displacement at the base of the ith column is u_i; the point R and the z axis move with displacement u_0; the displacement of the mass relative to the point R is u^r) (after Trifunac and Todorovska, 1997)

To include in the analysis the multi-storey buildings vibrating in their first natural mode, an equivalent SDOF system was analyzed (see Figure 16). After a detailed modal analysis, which took into account characteristic simplifications relevant to the multi-storey buildings, an additional parameter δ was added to the whole analysis. This parameter equals 1 for the one-storey structural model of Figure 15, while for a multi-storey building it depends on the number of its storeys as well as on the assumed shape of the 1st mode (sinusoidal or straight line). For example, δ is 0.15 for a 10-storey building with the first natural period $T_1 = 1$ s. Again, the respective response spectrum definition has a very simple form:

$$SDC(T_1, \delta, \xi, \tau) = \max_t \left[u^r(t)\delta + v(t)\tau - \tfrac{1}{2} a(t)\tau^2 \right] \tag{48}$$
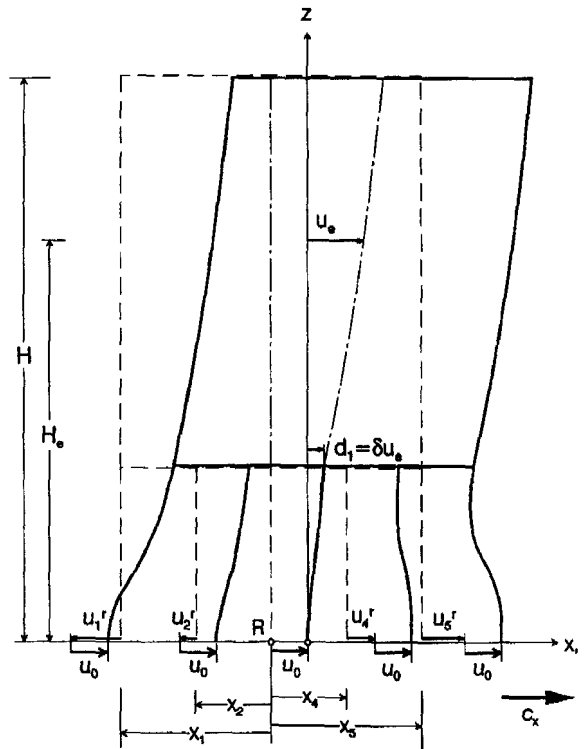

Fig. 16 A multi-storey building excited by asynchronous motion at the base of the first-storey columns (point R and the z axis move with the displacement u_0; u_C is the relative displacement of the equivalent SDOF oscillator excited by the acceleration $\ddot{u}_0(t)$, and d_1 is the relative displacement of the first storey) (after Trifunac and Todorovska, 1997)

The SDC spectra can be easily calculated from the existing earthquake records for specific values of δ characteristic of certain building types, with values of τ specified according to column configurations and wave patterns specific for particular ground conditions. Furthermore, as shown by Trifunac and Todorovska (1997), the SDC response spectrum (see Equation (48)) can effectively be approximated by the "square-root-of-sum-of-squares" rule as follows:

$$SDC(T_1, \delta, \xi, \tau) \approx \left[\delta^2 SD^2(T, \xi) + \left(v_{max}\tau \right)^2 - \left(\tfrac{1}{2} a_{max}\tau^2 \right)^2 \right]^{1/2} \tag{49}$$

where $SD(T, \xi)$ is the familiar displacement response spectrum while v_{max} and a_{max} denote the respective maxima of $v(t)$ and $a(t)$.

In Figure 17, the plots of the column differential response spectra for a one-storey structure ($\delta = 1$) and damping ratio $\xi = 0.05$ are illustrated for various values of τ, with solid lines denoting the application of Equation (48) and dashed lines denoting the approximation (as in Equation (49)). It is interesting to note the flat zones on the left side of Figure 17, in which the SDC response spectrum diverges from the classic displacement response spectrum. It shows the domination of the pseudo-static

component in the structural response for short-natural-period (stiff) buildings. This result can also be observed in the independently obtained plot of force spatial response spectrum as shown in Figure 5.
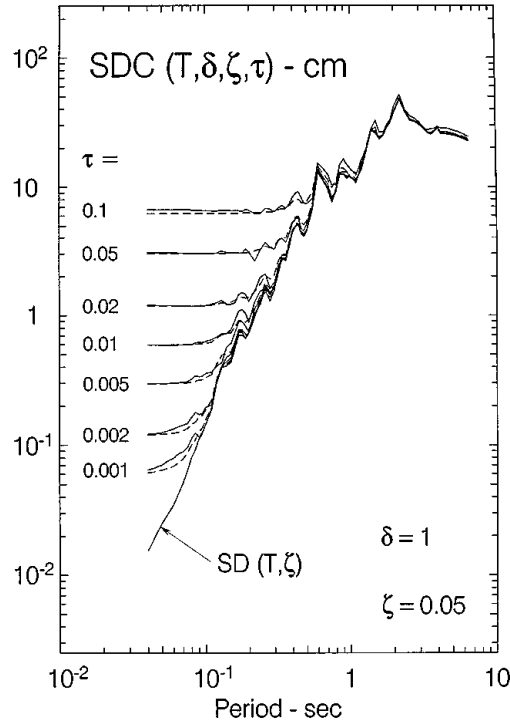

Fig. 17 In-plane building column response spectrum for the S16W component of the acceleration recorded at Station # 53 of the Los Angeles Strong Motion Network during the Northridge, CA, earthquake of 17 January 1994 ($M = 6.7$), at the epicentral distance of 6 km with $\xi = 0.05$ and $\delta = 1$ (one-storey building) (solid line is for Equation (48), and dashed-line approximation for Equation (49)) (after Trifunac and Todorovska, 1997)

2. Response Spectra for Differential, Out-of-plane Motion of Columns of a Building Structure

Figure 18 illustrates the model analyzed by Trifunac and Gicev (2006). In this case, the out-of-plane differential motion of columns, omitted in the analysis of the previous example, is analyzed. Such a motion can be caused by the passage of SH or Love waves among the columns of the structure. The analyzed two-degrees-of-freedom structural model is depicted in Figure 19. As for the in-plane motions, a reference point R is adopted. Its motion $u_0(t)$ (see Equation (46)) represents the ground motion averaged over the length of the structure L. In contrast to the previous example, this time the stiffness k_i works with the out-of-plane component of the motion (see Figure 19). The primary difference between the present and the previous example is the fact that this structural model has following two degrees of freedom:

- transversal motion of the rigid floor with mass m, and
- torsional motion of this floor about the vertical axis through R.

In the analysis presented by Trifunac and Gicev (2006), analogous assumptions are made, as in the paper of Trifunac and Todorovska (1997). In particular, an equivalent phase velocity c_{eq} is defined to represent both body and surface wave effects. Under conditions described by Trifunac and Gicev (2006), the two dynamic degrees of freedom are uncoupled, and the out-of-plane differential response spectra for the columns in the one-storey model of Figure 18 can be described by

$$SDC(T, T_T, \xi, \xi_T, \tau) = \max_t \left[u_r(t) + \Theta(t) x_i v(t) \tau - \tfrac{1}{2} a(t) \tau^2 \right] \tag{50}$$

where $u_r(t)$ and $\Theta(t)$ are the displacement and torsion of the rigid mass, respectively (see Figure 19), while $v(t)$ and $a(t)$ are the velocity and acceleration of the reference point R. The maxima of the above

four components of the SDC response spectrum occur generally at different time instants, which complicates the analysis. However, assuming that $\Theta_{\max} x_i \approx v_{\max} \tau_i$, neglecting the contribution of $a(t)$ (i.e., the term of Equation (42) with the multiplier, τ^2), and using, as previously, the "root-of-sum-of-squares" approximation, further simplifications can be made and the SDC spectrum can be approximated as

$$SDC(T, T_T, \xi, \xi_T, \tau) \approx \left[u_{r\max}^2 + 2\left(v_{\max}\tau\right)^2 \right]^{\frac{1}{2}} \tag{51}$$
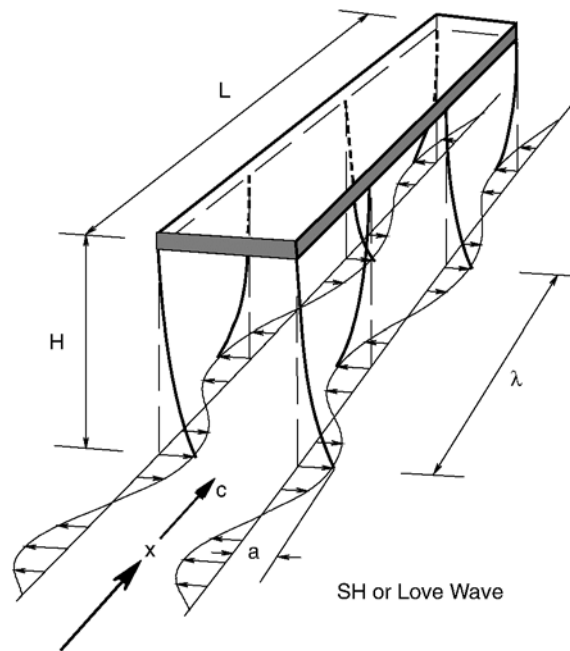
Fig. 18 One-storey structure excited by Love and/or SH waves propagating along its long dimension (after Trifunac and Gicev, 2006)
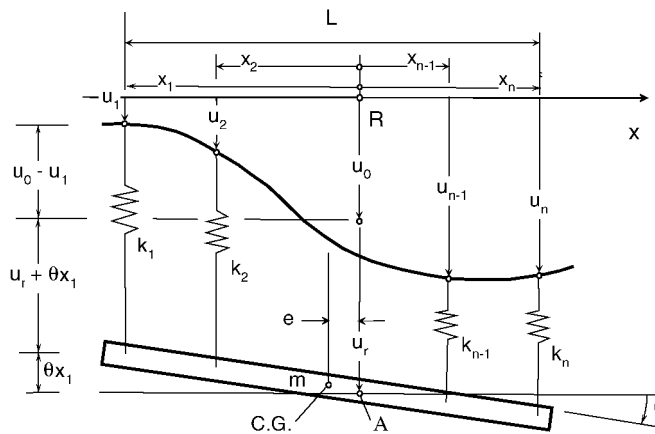
Fig. 19 Simplified 2-DOF model of the structure shown in Figure 18 (after Trifunac and Gicev, 2006)

The out-of-plane SDC spectrum can be generalized further to include, as in the previous example, the effects of differential ground motions on the first-storey columns of a multi-storey building responding in the first vibration mode. In this case, the torsional mode can be approximated by a straight line, and the SDC spectrum for the ith column becomes

$$SDC(T, T_T, \xi, \xi_T, \tau, \delta) = \max_t \left[\delta u_r(t) + \delta \Theta(t) x_i + v(t)\tau_i - \tfrac{1}{2} a(t)\tau_i^2 \right] \tag{52}$$

With further simplifications (Trifunac and Gicev, 2006), this response spectrum can be approximated by

$$SDC(T,T_T,\xi,\xi_T,\tau) \approx \left[\delta^2 SD^2\left(T,\xi\right) + \left(1+\delta\right)\left(v_{max}\tau_i\right)^2 \right]^{\frac{1}{2}} \tag{53}$$

To plot any of the above response spectra, a particular ratio between the transversal natural period T and the torsional period T_T should be established (for a typical building, T/T_T can be, for example, equal to $\sqrt{3} \approx 1.73$).

In Figure 20, the SDC spectrum calculated for a single-storey structural model ($\delta = 1$) is illustrated for various values of τ and compared with the ordinary displacement response spectrum. The solid lines in this figure represent the application of Equation (52), while the dashed lines denote the approximation as in Equation (53). On comparing the plots of Figure 20 with those of Figure 17 (longitudinal vibrations) it can be noted that they are quite similar but due to the additional contributions from torsional vibrations, the spectra in Figure 20 are larger than those in Figure 17.
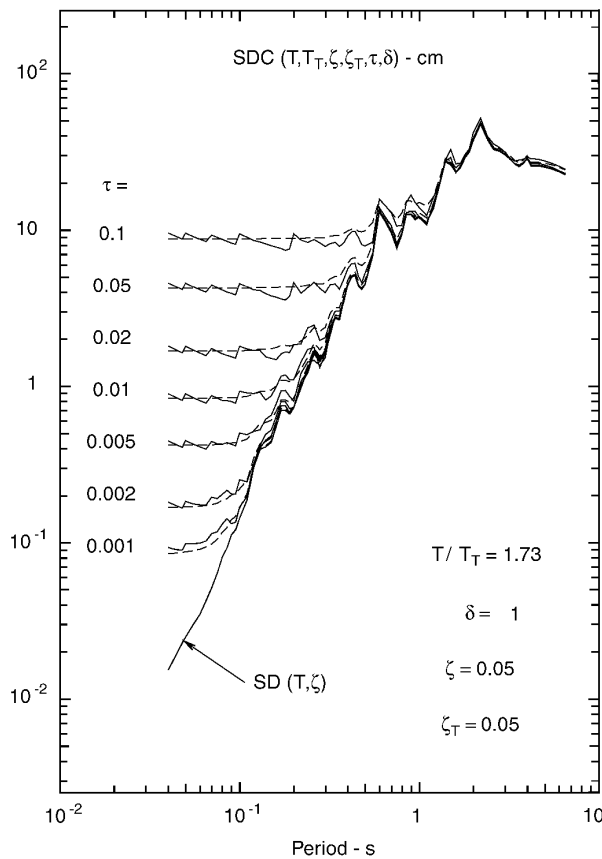

Fig. 20 Out-of-plane SDC response spectrum for the S16W component of the acceleration recorded at Station # 53 of the Los Angeles Strong Motion Network during the Northridge, CA, earthquake of 17 January 1994 ($M = 6.7$), at the epicentral distance of 6 km with $\xi = 0.05$ and $\delta = 1$ (one-storey building) (solid line is for Equation (52), and dashed-line approximation for Equation (53)) (after Trifunac and Gicev, 2006)

SUMMARY AND CONCLUSIONS

Examples of different extensions of the response spectrum method to include the consequences of spatial variations and of propagation of seismic waves were briefly reviewed. Two approaches were described in some detail: random vibrations of a simple SDOF system with two-component seismic excitations, and a multi-component column response spectrum for the multi-storey buildings.

While the random vibration approach is based on rational analyses of the seismic data from dense arrays of synchronized accelerometers (e.g., SMART-1), it actually does not allow in-depth analyses of the specific wave-passage effects due to temporal averaging included in the stochastic processing of the data. That is why the alternative approach using the waves propagating along the columns of a building sheds new light on the problem of spatial seismic effects on structures. It still requires approximations, but their validity can be carefully verified by analyzing a number of recent records of strong ground motion. In particular, it is interesting that such an intuitive, engineering notion as "apparent wave velocity" could also be derived from experimental wave-passage analyses as "equivalent phase velocity". Both approaches indicate the importance of the spatial seismic effects for the short-period stiff structures (see Figures 5, 17, and 20), but the differences in the local site effects can also be important (as shown in Figures 12–14), thus contributing further to the complexity of the problem.

The need for future research in this area should be apparent. Detailed analyses of wave passages, the role of group velocities of strong motion waves, and of the rotational components of seismic ground motion, will lead to the development of more detailed models of spatial seismic effects on structures. Modern suspension bridges may have their supports as far as 2 km apart (e.g., Akashi bridge in Japan), with the existing designs approaching a 3.3-km span (Messina bridge in Italy). In such cases, the effects of nonstationarity of spatial seismic random fields cannot be neglected. This and further refinements involving soil-structure interaction effects among the multi-support foundations will be the challenging new areas of research for future investigations.

ACKNOWLEDGEMENTS

APPENDIX I: POWER SPECTRAL DENSITY OF SEISMIC GROUND MOTION

The popular engineering model of power spectral density of the seismic accelerations was proposed by Kanai (1957) and Tajimi (1960):

$$S(\omega) = \frac{\omega_g^4 + (2\xi_g \omega_g \omega)^2}{(\omega_g^2 - \omega^2)^2 + (2\xi_g \omega_g \omega)^2} S_0 \tag{A.1}$$

The advantageous feature of the Kanai-Tajimi ground motion model is its ability to model local site effects by the frequency ω_g and damping ratio ξ_g, which can then be treated as the local soil parameters, while S_0 denotes the seismic intensity factor. Typical ranges for these parameters are: 2π to 6π rad/s for ω_g, and 0.2 to 0.6 for ξ_g. The Kanai-Tajimi spectrum takes an unrealistic non-zero value for $\omega = 0$. This undesirable effect has been corrected by introducing a high-pass filter, as proposed by Ruiz and Penzien (1969), leading to the following spectral density function:

$$S(\omega) = \frac{\omega_g^4 + (2\xi_g \omega_g \omega)^2}{(\omega_g^2 - \omega^2)^2 + (2\xi_g \omega_g \omega)^2} \frac{\omega^4}{(\omega_h^2 - \omega^2)^2 + (2\xi_h \omega_h \omega)^2} S_0 \tag{A.2}$$

in which $\omega_h = 1.636$ and $\xi_h = 0.619$ are the constants proposed by Ruiz and Penzien (1969).

REFERENCES

1. Abrahamson, N.A. and Bolt, B.A. (1985). "The Spatial Variation of the Phasing of Seismic Strong Ground Motion", Bulletin of the Seismological Society of America, Vol. 75, No. 5, pp. 1247–1264.

2. Abrahamson, N.A., Bolt, B.A., Darragh, R.B., Penzien, J. and Tsai, Y.B. (1987). "The SMART 1 Accelerograph Array (1980–1987): A Review", Earthquake Spectra, Vol. 3, No. 2, pp. 263–287.

3. Abrahamson, N.A., Schneider, J.F. and Stepp, J.C. (1991). "Empirical Spatial Coherency Functions for Application to Soil-Structure Interaction Analyses", Earthquake Spectra, Vol. 7, No. 1, pp. 1–27.

4. Aki, K. and Richards, P.G. (1980). "Quantitative Seismology: Theory and Methods", W.H. Freeman & Company, San Francisco, U.S.A.

5. Biot, M.A. (1932). "Transient Oscillations in Elastic Systems", Ph.D. Thesis No. 259, Aeronautics Department, California Institute of Technology, Pasadena, U.S.A.

6. Biot, M.A. (1941). "A Mechanical Analyzer for the Prediction of Earthquake Stresses", Bulletin of the Seismological Society of America, Vol. 31, No. 2, pp. 151–171.

7. Bycroft, G.N. (1983). "Differential-Ground-Motion Array at Hollister Municipal Airport, California", Open-File Report 83-327, United States Geological Survey, Denver, U.S.A.

8. Datta, T.K. (1999). "Seismic Response of Buried Pipelines: A State-of-the-Art Review", Nuclear Engineering and Design, Vol. 192, No. 2-3, pp. 271–284.

9. Der Kiureghian, A. (1980). "Structural Response to Stationary Excitation", Journal of the Engineering Mechanics Division, Proceedings of ASCE, Vol. 106, No. EM6, pp. 1195–1213.

10. Der Kiureghian, A. (1981). "A Response Spectrum Method for Random Vibration Analysis of MDF Systems", Earthquake Engineering & Structural Dynamics, Vol. 9, No. 5, pp. 419–435.

11. Der Kiureghian, A. (1996). "A Coherency Model for Spatially Varying Ground Motions", Earthquake Engineering & Structural Dynamics, Vol. 25, No. 1, pp. 99–111.

12. Der Kiureghian, A. and Neuenhofer, A. (1992). "Response Spectrum Method for Multi-Support Seismic Excitations", Earthquake Engineering & Structural Dynamics, Vol. 21, No. 8, pp. 713–740.

13. Dulinska, J. and Zieba, A. (2007). "The Effect of Mine Shocks and Quarry Blasts on Dynamic Response of a Gas Pipeline", Czasopismo Techniczne, Cracow University of Technology, Vol. 104, No. 2-B/6, pp. 19–27 (in Polish).

14. Gupta, I.D. and Trifunac, M.D. (1998). "Defining Equivalent Stationary PSDF to Account for Nonstationarity of Earthquake Ground Motion", Soil Dynamics and Earthquake Engineering, Vol. 17, No. 2, pp. 89–99.

15. Hao, H. (1989). "Effects of Spatial Variation of Ground Motions on Large Multiply-Supported Structures", Report UCB/EERC-89/06, University of California, Berkeley, U.S.A.

16. Hao, H. (1991). "Response of Multiply Supported Rigid Plate to Spatially Correlated Seismic Excitations", Earthquake Engineering & Structural Dynamics, Vol. 20, No. 9, pp. 821–838.

17. Harichandran, R.S. and Vanmarcke, E.H. (1986). "Stochastic Variation of Earthquake Ground Motion in Space and Time", Journal of Engineering Mechanics, ASCE, Vol. 112, No. 2, pp. 154–174.

18. Harichandran, R.S. and Wang, W. (1988). "Response of Simple Beam to Spatially Varying Earthquake Excitation", Journal of Engineering Mechanics, ASCE, Vol. 114, No. 9, pp. 1526–1541.

19. Harichandran, R.S. and Wang, W. (1990). "Response of Indeterminate Two-Span Beam to Spatially Varying Seismic Excitation", Earthquake Engineering & Structural Dynamics, Vol. 19, No. 2, pp. 173–187.

20. Hindy, A. and Novak, M. (1980). "Pipeline Response to Random Ground Motion", Journal of the Engineering Mechanics Division, Proceedings of ASCE, Vol. 106, No. EM2, pp. 339–360.

21. Kanai, K. (1957). "Semi-Empirical Formula for the Seismic Characteristics of the Ground", Bulletin of the Earthquake Research Institute, University of Tokyo, Vol. 35, pp. 309–325.

22. Kojic, S. and Trifunac, M.D. (1991a). "Earthquake Stresses in Arch Dams. I: Theory and Antiplane Excitation", Journal of Engineering Mechanics, ASCE, Vol. 117, No. 3, pp. 532–552.

23. Kojic, S. and Trifunac, M.D. (1991b). "Earthquake Stresses in Arch Dams. II: Excitation by SV, P and Rayleigh Waves", Journal of Engineering Mechanics, ASCE, Vol. 117, No. 3, pp. 553–574.

24. Leger, P., Ide, M.I. and Paultre, P. (1990). "Multiple-Support Seismic Analysis of Large Structures", Computers & Structures, Vol. 36, No. 6, pp. 1153–1158.

25. Loh, C.H., Penzien, J. and Tsai, Y.B. (1982). "Engineering Analyses of SMART 1 Array Accelerograms", Earthquake Engineering & Structural Dynamics, Vol. 10, No. 4, pp. 575–591.

26. Luco, J.E. and Wong, H.L. (1986). "Response of a Rigid Foundation to a Spatially Random Ground Motion", Earthquake Engineering & Structural Dynamics, Vol. 14, No. 6, pp. 891–908.

27. Novak, M. (1990). "Spatial Correlation Effects in Random Vibration of Structures", Proceedings of the European Conference on Structural Dynamics, EURODYN'90, Bochum, F.R.G., Vol. 2, pp. 631–636.

28. Perotti, F. (1990). "Structural Response to Non-stationary Multiple-Support Random Excitation", Earthquake Engineering & Structural Dynamics, Vol. 19, No. 4, pp. 513–527.

29. Roesset, J.M. (1977). "Soil Amplification of Earthquakes" in "Numerical Methods in Geotechnical Engineering (edited by C.S. Desai and J.T. Christian)", McGraw-Hill, New York, U.S.A.

30. Ruiz, P.T. and Penzien, J. (1969). "Probabilistic Study of the Behavior of Structures during Earthquakes", Report UCB/EERC-69/03, University of California, Berkeley, U.S.A.

31. Safak, E. (1995). "Discrete-Time Analysis of Seismic Site Amplification", Journal of Engineering Mechanics, ASCE, Vol. 121, No. 7, pp. 801–809.

32. Shinozuka, M. and Deodatis, G. (1991). "Stochastic Wave Models for Stationary and Homogeneous Seismic Ground Motion", Structural Safety, Vol. 10, No. 1-3, pp. 235–246.

33. Tajimi, H. (1960). "A Statistical Method of Determining the Maximum Response of a Building Structure during an Earthquake", Proceedings of the Second World Conference on Earthquake Engineering, Tokyo, Japan, Vol. 2, pp. 781–798.

34. Todorovska, M.I. and Lee, V.W. (1989). "Seismic Waves in Buildings with Shear Walls or Central Core", Journal of Engineering Mechanics, ASCE, Vol. 115, No. 2, pp. 2669–2686.

35. Todorovska, M.I. and Trifunac, M.D. (1989). "Antiplane Earthquake Waves in Long Structures", Journal of Engineering Mechanics, ASCE, Vol. 115, No. 12, pp. 2687–2708.

36. Todorovska, M.I. and Trifunac, M.D. (1990a). "A Note on the Propagation of Earthquake Waves in Buildings with Soft First Floor", Journal of Engineering Mechanics, ASCE, Vol. 116, No. 4, pp. 892–900.

37. Todorovska, M.I. and Trifunac, M.D. (1990b). "Note on Excitation of Long Structures by Ground Waves", Journal of Engineering Mechanics, ASCE, Vol. 116, No. 4, pp. 952–964.

38. Todorovska, M.I. and Trifunac, M.D. (1997). "Amplitudes, Polarity and Time of Peaks of Strong Ground Motion during the 1994 Northridge, California, Earthquake", Soil Dynamics and Earthquake Engineering, Vol. 16, No. 4, pp. 235–258.

39. Todorovska, M.I., Hayir, A. and Trifunac, M.D. (2001a). "Antiplane Response of a Dike with Flexible Structure-Soil Interface to Incident SH-Waves", Soil Dynamics and Earthquake Engineering, Vol. 21, No. 7, pp. 603–613.

40. Todorovska, M.I., Hayir, A. and Trifunac, M.D. (2001b). "Antiplane Response of a Dike on a Flexible Embedded Foundation to Incident SH-Waves", Soil Dynamics and Earthquake Engineering, Vol. 21, No. 7, pp. 593–601.

41. Trifunac, M.D. (1971). "Response Envelope Spectrum and Interpretation of Strong Earthquake Ground Motion", Bulletin of the Seismological Society of America, Vol. 61, No. 2, pp. 343–356.

42. Trifunac, M.D. (1990). "How to Model Amplification of Strong Earthquake Motions by Local Soil and Geologic Site Conditions", Earthquake Engineering & Structural Dynamics, Vol. 19, No. 6, pp. 833–846.

43. Trifunac, M.D. (1997). "Relative Earthquake Motion of Building Foundations", Journal of Structural Engineering, ASCE, Vol. 123, No. 4, pp. 414–422.

44. Trifunac, M.D. and Gicev, V. (2006). "Response Spectra for Differential Motion of Columns. Paper II: Out-of-Plane Response", Soil Dynamics and Earthquake Engineering, Vol. 26, No. 12, pp. 1149–1160.

45. Trifunac, M.D. and Lee, V.W. (1996). "Peak Surface Strains during Strong Earthquake Motion", Soil Dynamics and Earthquake Engineering, Vol. 15, No. 5, pp. 311–319.

46. Trifunac, M.D. and Todorovska, M.I. (1997). "Response Spectra for Differential Motion of Columns", Earthquake Engineering & Structural Dynamics, Vol. 26, No. 2, pp. 251–268.

47. Trifunac, M.D., Todorovska, M.I. and Ivanovic, S.S. (1996). "Peak Velocities and Peak Surface Strains during Northridge, California, Earthquake of 17 January 1994", Soil Dynamics and Earthquake Engineering, Vol. 15, No. 5, pp. 301–310.

48. Vanmarcke, E.H. and Fenton, G.A. (1991). "Conditioned Simulation of Local Fields of Earthquake Ground Motion", Structural Safety, Vol. 10, No. 1-3, pp. 247–264.

49. Zembaty, Z. (1996). "Spatial Seismic Coefficients, Some Sensitivity Results", Journal of Engineering Mechanics, ASCE, Vol. 122, No. 4, pp. 379–382.

50. Zembaty, Z. (1997). "Vibrations of Bridge Structure under Kinematic Wave Excitations", Journal of Structural Engineering, ASCE, Vol. 123, No. 4, pp. 479–488.

51. Zembaty, Z. and Krenk, S. (1993). "Spatial Seismic Excitations and Response Spectra", Journal of Engineering Mechanics, ASCE, Vol. 119, No. 12, pp. 2449–2460.

52. Zembaty, Z. and Rutenberg, A. (1998). "On the Sensitivity of Bridge Seismic Response with Local Soil Amplification", Earthquake Engineering & Structural Dynamics, Vol. 27, No. 10, pp. 1095–1099.

53. Zembaty, Z. and Rutenberg, A. (2002). "Spatial Response Spectra and Site Amplification Effects", Engineering Structures, Vol. 24, No. 11, pp. 1485–1496.

54. Zerva, A. (1991). "Effect of Spatial Variability and Propagation of Seismic Ground Motions on the Response of Multiply Supported Structures", Probabilistic Engineering Mechanics, Vol. 6, No. 3-4, pp. 212–221.

55. Zerva, A. and Shinozuka, M. (1991). "Stochastic Differential Ground Motion", Structural Safety, Vol. 10, No. 1-3, pp. 129–143.